Earthq Eng & Eng Vib (2021) 20: 361-375 **DOI**: https://doi.org/10.1007/s11803-021-2025-8

Behavior of braced wall embedded in saturated liquefiable sand under seismic loading

Sanku Konai†, Aniruddha Sengupta‡ and Kousik Deb§

Department of Civil Engineering, Indian Institute of Technology Kharagpur, Kharagpur 721302, India

Abstract: It is well known that the generation of excess pore water pressure and/or liquefaction in foundation soils during an earthquake often cause structural failures. This paper describes the behavior of a small-scale braced wall embedded in saturated liquefiable sand under dynamic condition. Shake table tests are performed in the laboratory on embedded retaining walls with single bracing. The tests are conducted for different excavation depths and base motions. The influences of the peak magnitude of the ground motions and the excavation depth on the axial forces in the bracing, the lateral displacement and the bending moments in the braced walls are studied. The shake table tests are simulated numerically using FLAC 2D and the results are compared with the corresponding experimental results. The pore water pressures developed in the soil are found to influence the behavior of the braced wall structures during a dynamic event. It is found that the excess pore water pressure development in the soil below the excavation is higher compared to the soil beside the walls. Thus, the soil below the excavation level is more susceptible to the liquefaction compared to the soil beside the walls.

Keywords: braced wall; FLAC 2D; liquefaction; seismic analysis; shake table test

1 Introduction

In congested modern cities, deep vertical excavation is done quite frequently for the construction of underground transportation tunnels, laying out utility pipe lines and for the construction of the foundation and the basements for a high-rise building. A deep vertical excavation is often supported by retaining walls and the horizontal member or bracing system is provided to resist the lateral thrust on the walls. The sheet pile walls are often used as retaining walls for temporary construction or they might be reinforced concrete walls, if the construction is permanent in nature as in the case of an underground metro rail station. The bracing system often consists of wales and struts. The wales are steel beams designed to transfer the loads coming from the soil to the steel struts through the retaining wall. The struts are steel or concrete beams designed to resist longitudinal compression, which can be used to maintain the opening/ excavation between two retaining walls. Extensive research has been conducted on braced walls and excavations under static condition through numerous theoretical and/or physical models (Finno *et al*., 1991; Finno and Harahap, 1991; Bose and Som, 1998; Nakai *et al*., 1999; Long, 2001; Liu *et al*., 2005; Karlsrud and Andresen, 2005; Wang *et al*., 2005, Tefera *et al*., 2006; Kung *et al*., 2007; Hsiung, 2009; Chowdhury *et al*., 2013, 2016, 2017). The seismic performance of this type of wall, being temporary in nature most of the time, is not investigated thoroughly. However, presently, due to complications arising from land acquisition, litigations, etc., these constructions go on for years and their performance during earthquake conditions need to be reviewed, if located in a seismic prone area. Several numerical and experimental analyses on braced excavations in dry sand have been performed considering seismic loading conditions (Callisto *et al*., 2008; Conti *et al*., 2012; Chowdhury *et al*., 2015, Konai *et al*., 2017, 2018). Very recently, studies are also performed by various researchers on retaining or embedded wall, excavation and other types of structures under seismic condition (Chen *et al.,* 2017; Pain *et al*., 2017; Zhou *et al*., 2017; Zhao *et al*., 2017; Aminpour *et al*., 2018; Xie *et al*., 2018; Gu *et al*., 2018; Gu *et al*., 2018; Tavakoli *et al*., 2019; Konai *et al*., 2020). Zeng (2005) conducted centrifuge tests on soil liquefaction on anchored sheet pile walls. The stiffness of the soil-wall system is found to decrease due to soil liquefaction, which in turn could cause amplification of the seismic vibration. Zekri *et al*. (2015) investigated the seismic behavior of anchored sheet pile wall in liquefiable soil. A remediation method involving soil compaction is used to improve the behavior of the anchored sheet pile wall in dynamic conditions. Tricarico *et al*. (2016) carried

Correspondence to: Kousik Deb, Department of Civil Engineering, Indian Institute of Technology Kharagpur, Kharagpur 721302, India
Tel: +91-3222-283434; Fax: +91-3222-98032
E-mail: kousik@civil.iitkgp.ac.in
†Former Research Scholar; ‡Professor; §Associate Professor

Supported by: Grant No. SR/S3/MERC-0029/2011 of SERB, Department of Science & Technology, New Delhi, India
Received June 5, 2019; **Accepted** April 4, 2020

out centrifuge model tests on flexible propped and cantilever retaining walls in saturated sand subjected to sinusoidal dynamic loadings. Their results showed that as far as amplification of wave is concerned, there is significant difference if the sand is dry or saturated. It may be observed that the accumulated displacement is higher in the saturated sand due to the generation of pore water pressures. It is noticed that most of the studies on flexible retaining structures or bracing systems are conducted under static conditions. The studies under seismic conditions are conducted mainly on dry sand. Very limited studies are conducted on braced walls embedded in saturated liquefiable sand under seismic loadings. The development of pore water pressures and lateral earth pressures, and their influences on a braced wall subjected to seismic loadings, is still not properly understood and a detailed investigation is required to understand the behavior of a braced wall under dynamic load conditions, if the surrounding soil is saturated and liquefies during a seismic event. The endeavor of the present investigation is to understand the performance of a braced wall embedded in fully saturated liquefiable sand under cyclic loading conditions. A number of shake table tests with a pair of small-scale model braced walls with a single bracing are conducted in the laboratory. In the experimental studies, the peak magnitude of the base motions and the depth of excavation are varied and the deformation, strain and forces acting on the structure along with the development of pore water pressures in the soil are measured. A numerical analysis using commercial software, FLAC 2D (Itasca, 2005), is also performed to understand the performance of the small-scale braced walls under the same sinusoidal seismic loadings. The results from the numerical and the experimental analyses are compared and presented in this paper.

2 Experimental program

The dynamic performance of a braced excavation in saturated sand supported by a pair of model braced walls with one level of bracing is investigated by laboratory shake table tests. Several researchers (Iai, 1989; Qiao *et al*., 2008; Ye *et al*., 2013; Ha *et al*., 2011) have utilized shake table tests to understand the behaviors of saturated sand under dynamic loading conditions. The tests are also utilized to study the soil-structure interaction under dynamic conditions (Koseki *et al*., 1998; Matsuo *et al*., 1998; Moghadam *et al*., 2011; Giri and Sengupta, 2009). The shake table comprises a rail mounted 1 m× 1 m steel table. The table is shaken in the horizontal direction only by a servo hydraulic actuator. The present model tests are done within a 0.8 m×0.885 m× 0.6 m (length×breadth×height) rigid plexiglass tank. The 16 mm thick plexiglass sheets are fixed in a steel frame with steel angles. The absorbing pads, made of thermocol sheets, are glued to the boundary walls of the test tank to prevent reflection of waves at the boundaries. Figure 1 shows a schematic diagram of a standard braced excavation problem (where H is the total depth of the retaining walls, Z is the total depth of the soil layer, B is the excavation width, s is the depth of the strut from the ground surface, t_w is the thickness of the retaining walls, and d is the depth from the ground line). In all the tests, the total depth of the retaining wall (H) is kept as 200 mm and the total depth of the soil layer (Z) is 400 mm. The excavation width (B) is kept constant at 160 mm for all the tests as it may affect the performance of the braced walls (Callisto and Soccodato, 2007). The embedded braced walls are modeled by two 2.4 mm thick plexiglass sheets. The two walls are kept apart by one level of bracing or strut located between the walls. The bracing or strut is a beam made of plexiglass and with a cross section of 12 mm × 12 mm. The values of the elastic modulus and the density of the plexiglass are 6.3×10^9 Pa and 1010 kg/m^3, respectively. The retaining walls and the strut are pin-jointed.

All the model tests are 1-g in nature (Iai, 1989) (small-scale model), where the values of the prototype and the model accelerations are kept same. The density of the model soil and that of the prototype soil is also the same. To convert the results from the model scale test to the prototype scale, 1-g scaling laws governing the dynamic problems can be used. The details regarding the 1-g scaling laws can be found in Meymand (1998), Wood (2004), Moghadam *et al*. (2011), and Bandyopadhyay *et al*. (2015). Considering a scale factor of 50 and using the 1-g scaling laws proposed by Meymand (1998), the representative prototype excavation depth is found to be 5 m. The length and the thickness of the prototype concrete (M25) braced wall are 10 m and 300 mm, respectively. A prototype strut may be a 200 mm thick continuous slab or a concrete beam (M25) of cross section 0.8 m ×0.8 m, if the plan distance or spacing between the two props or struts is 3 m.

The sand utilized in the tests is collected from a local river (Kasai River) near Kharagpur (West Bengal, India). The sand is uniformly grained and classified as poorly graded sand (SP) as per the Unified Soil

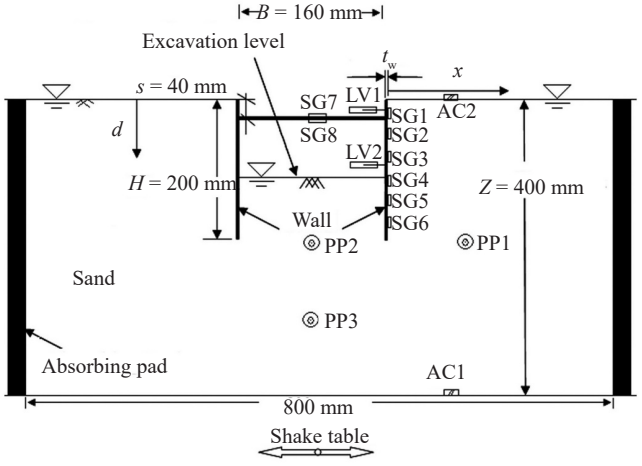

Fig. 1 Schematic diagram of the test setup

Classification System (USCS). Figure 2 shows the grain size distribution of the sand along with the boundaries proposed by Tsuchida (1970) for potentially liquefiable soils and most liquefiable soils. It may be seen from Fig. 2 that the Kasai River sand used in this study is located within the range of liquefiable soil. Thus, the sand used in this study is susceptible to liquefaction. The specific gravity of the sand (G_{sand}) is measured as 2.67. The maximum dry unit weight, $\gamma_{d(max)}$, and the minimum dry unit weight, $\gamma_{d(min)}$, are 16.7 kN/m^3 and 14.13 kN/m^3, respectively. The coefficient of curvature (C_c) and the uniformity coefficient (C_u) of the sand are found to be 0.87 and 2.84, respectively. To obtain the shear strength parameters of the sand, laboratory drained tri-axial tests are performed under different confining pressures. The effective peak and the constant volume angle of friction (φ') are 38° and 33°, respectively. The effective cohesion of the sand is 0.

In the model tests, the density and the water content of the sand are kept uniform with depth. This is very necessary as the liquefaction of a soil depends on the soil preparation method (Mullins *et al*., 1977). The preparation of a saturated soil bed is a difficult process in such testing, and that soil fabric may be locally remolded, disturbing the initial target state (relative density, etc.). Moreover, some air bubbles may appear (and remain) and the soil may locally not be fully saturated. Thus, a saturated soil sample is prepared very carefully. The dry sand is poured in the test chamber in four layers of 100 mm each and compacted maintaining a density of 1600 kg/m^3 (15.7 kN/m^3) and a relative density, D_r, of 65%. Initially, the dry sand is poured in two layers and compacted up to 200 mm height. After this, the model braced walls with the struts are placed and the sand filling and the compaction continued until the top of the braced walls (400 mm in height) is reached. The sand around the braced walls and within the two walls is hand compacted (tampered) to the same density. After the compaction and the filling are complete, the required amount of water is added to the soil for complete saturation. Considering the degree of saturation (S) as unity, the required water content (w) is found to be 25.09% to achieve the full saturation of the soil (using $wG_{sand} = eS$, where e is the void ratio of the sand=0.67). The density and the void ratio of the sand bed are rechecked from the random samples obtained from the sand bed after its construction. The soil in between the two retaining walls is then removed up to a depth, D_e, from the top. During the tests, the phreatic level is maintained just below the excavation level by a continuous dewatering process (by pumping out the water) from the excavated area. At the same time, a continuous supply of water is also fed into the ground surface to keep the phreatic level at the top surface outside the excavation area. A steady state, static pressure is maintained before the shaking. Three pore water pressure transducers are utilized to monitor the development of pore water pressures in the sand bed during the shaking. Figure 3 shows the whole laboratory test setup. This whole setup is then subjected to horizontal shaking by specifying the amplitude and the frequency of a predetermined motion to the actuator attached to the shake table.

In this study, six strain gauges (SG1-6) are attached to the right retaining wall at 15 mm, 60 mm, 95 mm, 110 mm, 150 mm and 170 mm from the top of the wall and two strain gauges (SG7, SG8) are attached to one of the struts. Two linearly variable differential transformers (LVDTs) (LV1 and LV2) are attached at 15 mm and 60 mm from the top of the wall as shown in Fig. 1. The LVDTs used in the experiments have a least count of 0.01 mm and have a maximum measuring capacity of 20 mm (±10 mm). The lateral displacements of the retaining wall after a dynamic event are calculated from the LVDT measurements and by double integrating the obtained equation of the curvature along the length of the wall. The equation of curvature is obtained from the readings of the strain gauges, which are attached to the wall (SG1-6). The LVDT measurements are used as boundary conditions during the integration to determine the lateral displacements of the wall. The bending moments in the retaining wall are back calculated from the readings of the strain gauges. The axial forces in the struts, that is, the strut forces (F), are also calculated from the readings of the strain gauges, SG7 and SG8. The developed strains

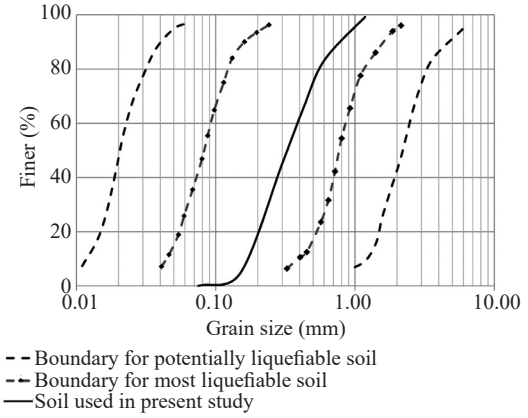

Fig. 2 Grain size distribution of the sand used in the present study and the boundaries of liquefaction susceptible soils proposed by Tsuchida (1970)

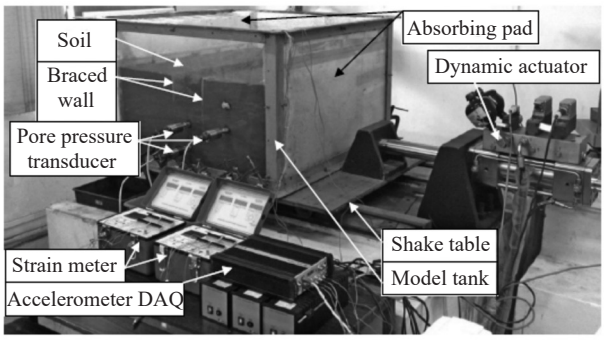

Fig. 3 Laboratory shake table test on braced excavation

in the struts during an event are multiplied with $E_p A$ of the strut to obtain the strut forces where E_p is the Young′s modulus and A is the cross-sectional area of a strut. The accelerometers, AC1and AC2, are placed at the bottom and the top of the soil layer (see Fig. 1). Three pore pressure transducers (PP1, PP2 and PP3) are attached to the model tank for measuring the pore pressures that developed within the soil during a test. PP1 is placed 200 mm (1H) from the top soil surface and 100 mm (0.5H) away from right wall (as shown in Fig. 1). PP2 and PP3 are placed 100 mm (0.5H) and 200 mm (1H) below the level of excavation, respectively, and in the middle of the excavation width (B) (refer to Fig. 1). The bottom stability of the excavation between the braced walls and the stability (kick out) of the toe of the walls are important concerns during liquefaction. Thus, the pore water pressure transducers are placed below the excavation and at the toe of the wall. The pore water pressures measured during the model tests also indicate that the initiation of liquefaction starts from the bottom of the excavation. Two accelerometers, AC1 and AC2, are recorded at 20 data per second during shaking. The pore pressure measurements at PP1, PP2 and PP3 are recorded at one data per second. The readings from the LVDTs (LV1 and LV2) and the strain gauges (SG1-6 for wall and SG7-8 for strut) are taken at the beginning (initial data) and at the end (final data) of the shaking. The net post seismic responses of the right braced wall are studied to show the performance of the braced excavation only due to the seismic loading.

3 Selected motions

In all the shake table experiments, sinusoidal motions are imparted to the table and the test set up with the magnitude of the acceleration between 0.15 g to 0.35 g (refer to Table 1) to cover for most of the common cases. As per the seismic zonation map of India (IS:1893, 2002) and other published (Dasgupta *et al*., 2000) seismic maps of India, most of the seismically active part of the Indian plateau may experience an earthquake with peak ground acceleration between 0.15 g and 0.35 g. Thus, the magnitude of acceleration between 0.15 g to 0.35 g is selected in the present study to cover for most of the major cities within India.The 14 cycles of sinusoidal motions at a frequency of 2 Hz are applied for each test. A typical sinusoidal motion considered in the study (for the case of BW2) is shown in Fig. 4. The applied motions to the actuator are found to be almost same as those measured at AC1. Thus, the motions specified to the actuator are also specified as the base motions for the numerical analysis. BW2 is considered as the reference test for this study, which is conducted with 0.25 g peak amplitude of base acceleration and D_e/H = 0.5. Then, keeping the other properties and conditions identical, peak acceleration is varied from 0.15 g to 0.35 g for the BW1 and BW3 tests. Similarly, keeping all the other conditions identical, D_e/H is varied from 0.4 to 0.6 for the BW4 and BW5 tests. These parametric studies are carried out understand the effects of peak amplitude of base accelerations and depth of excavations on the behavior of braced excavation.

4 Numerical analysis

The shake table tests are numerically simulated using the commercial program FLAC 2D (Itasca, 2005). FLAC 2D is based on the finite difference method assuming a 2D plane strain condition. The small-scale 2-D model of the braced walls along with the surrounding soil with the width in the horizontal direction of 800 mm and the depth (Z) of 400 mm is considered in the numerical analyses. The bottom boundary is considered immovable in both the x and y directions. The side boundaries are considered to be fixed in the horizontal direction and for the dynamic load cases, a free field condition is assumed as absorbing pads made of thermocol sheets and are glued to the walls of the test container. It is true that this absorbing pad is not 100% effective in eliminating the wave reflection, but Lombardi *et al*. (2015) have shown that the use of such soft material as an absorbing pad in the boundaries in a dynamic test can significantly reduce the reflection of waves at the boundaries. In the numerical analyses, the two extreme vertical boundaries are attached to the free field with the help of a viscous dashpot to obtain the boundaries. Figure 5 shows the numerical discretization of the braced excavation. A hyperbolic relationship is used to determine the Young′s modulus of the soil (for 1-g model) with depth from the laboratory tri-axial test data as (Janbu, 1963):

$$E_s = P_{ref} K_d \left[\frac{(\sigma'_m)}{P_{ref}} \right]^n \tag{1}$$

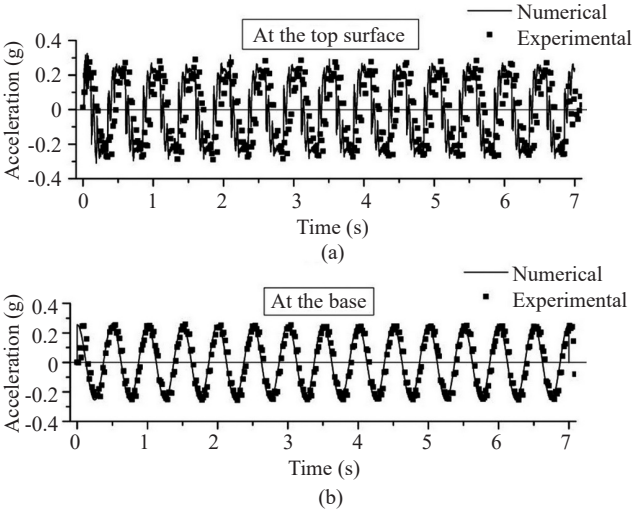

Fig. 4 Acceleration time history (a) at the top of the soil behind the braced wall (AC2) (b) at the bottom of the soil (AC1) for BW2 model test

Table 1 List of shake table tests on braced excavation in saturated sand

Test Name	Excavation Depth D_e (mm)	Embedment depth D_b (mm)	Normalized excavation depth D_e/H	Depth of the strut from top s (mm)	Wall thickness t_w (mm)	Total depth of the soil layer Z (mm)	Excavation width B (mm)	Maximum amplitude of the base acceleration
BW1	100	100	0.5	40	2.4	400	160	0.15 g
BW2	100	100	0.5	40	2.4	400	160	0.25 g
BW3	100	100	0.5	40	2.4	400	160	0.35 g
BW4	80	120	0.4	40	2.4	400	160	0.25 g
BW5	120	80	0.6	40	2.4	400	160	0.25 g

Note: BW means braced wall

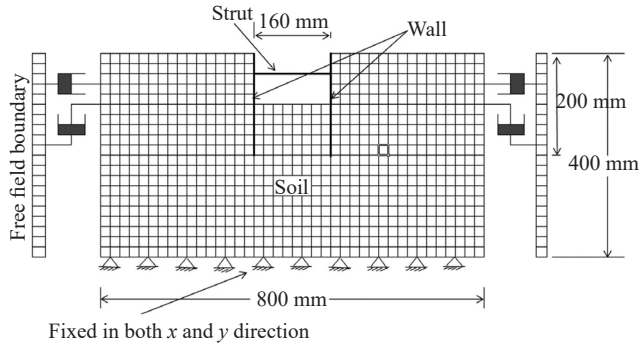

Fig. 5 Numerical discretization of the braced excavation

where P_{ref}=100 kPa, σ'_m = effective mean confining pressure. K_d and n are the two hyperbolic material parameters whose values are 402 and 0.5, respectively, obtained from the laboratory tri-axial test data. The shear modulus (G) and the bulk modulus (K) of the sand used in the numerical analyses are obtained from the well-known relationships $G=E_s/2(1+\mu_s)$ and $K=E_s/3(1-2\mu_s)$, where μ_s is the Poisson's ratio (=0.3) of the sand. The coefficient of lateral earth pressure at rest (K_0) is computed using the well-known relationship K_0 =1-sinφ' and found to be 0.38. The retaining walls and the struts are modeled by elastic beam elements and the connections between a strut and the retaining walls are considered as pin-jointed in the numerical analyses. For the plane strain analyses, the elastic modulus of the plexiglass walls used in the shake table tests is computed as $E_{pp}=E_p/(1-\mu_p^2)$, where the elastic modulus of the plexiglass (E_p) is taken as 6.3×10^9 N/m^2 and the Poisson ratio (μ_p) of the material is taken as 0.35. The interface elements are assumed in the numerical discretization between the structural (walls) elements and the soil elements to maintain the compatibility. The interface angle between the soil and the walls is assumed as 20°. The normal and the shear stiffnesses (K_n and K_s) at the soil-structure interfaces play a major role for predicting the behavior of the braced walls in a numerical analysis (Hsiung, 2009). The value of these stiffnesses, used in the analyses, is 3.3×10^9 Pa, which is calculated using Eq. (2) (Itasca, 2005) as:

$$K_n = K_s = 10 \times \left[\frac{\left(K + \frac{4}{3} G \right)}{\Delta z_{min}} \right] \quad (2)$$

where K, G and Δz_{min} are bulk and shear modulii of the soil and the smallest width of the adjacent zone in the soil (20 mm) in the perpendicular direction to the interface, respectively. As per Itasca (2005), the values of interface stiffnesses, K_n and K_s are considered to be equal. A similar method is also followed to find K_n and K_s for interface modeling of such problems in FLAC 2D by Chowdhury *et al.* (2013, 2015). Table 2 summarizes all the parameters and their values. The shear modulus value shown in Table 2 is the average value of the 200 mm soil layer (surrounding the wall). The G value of 1.66 MPa is calculated for the 1-g model under very low confining pressures. Thus, a low value of stiffness is considered in the numerical analyses.

The shear wave velocity (C_s) of the soil is determined as 29 m/s from Eq. (3), where the values of the small strain shear modulus (G_0), unit weight (γ) of soil are taken from Table 2. According to FLAC-2D (Itasca, 2005), the wavelength (λ) may be calculated using Eq. (5). The value of Δl, the spatial element size (or mesh size) is 0.02 m. The value of the maximum frequency f_{max} with which a seismic wave propagates through a soil is obtained as 145 Hz from Eq. (5). For the present study, the applied seismic motions have a frequency of 2 Hz for all the cases, which is far lower than the value of f_{max}. This ensures that the applied seismic wave propagates smoothly through the soil. In addition, the maximum lateral displacement of a wall for different mesh sizes (0.04 m, 0.02 m and 0.01 m) is also studied. The change in the maximum lateral displacement of the wall is less than 1%, when the mesh size is reduced from 0.02 to 0.01 m. Thus, in the present study, the surrounding soil is discretized by square elements of 20 mm × 20 mm in size.

$$C_s = \sqrt{\frac{G_0}{\rho}} = \sqrt{\frac{G_0 g}{\gamma}} \quad (3)$$

$$\lambda = 10\Delta l \tag{4}$$

$$f_{\max} = \frac{C_s}{\lambda} \tag{5}$$

where C_s is the shear wave velocity, ρ is the density of the soil, γ is the unit weight of the soil, G_0 is the small strain shear modulus, g is acceleration due to gravity, λ is the wavelength, Δl is the spatial element size (or mesh size) and $f_{\max}$ is the maximum frequency of the seismic wave that can propagate through the soil.

For the initial stages in the static simulations, the engineering behaviors of the sand are modeled by the Mohr-Coulomb constitutive model and a static analysis is performed where the gravity force is turned on and the whole system is allowed to equilibrate under its own (gravity) load. The actual construction sequences of the braced wall installation in the field are not followed in the laboratory model tests. The braced walls and the struts are assumed to be in place. Only the excavation of the soil and the dewatering between the braced walls are considered in this study. Thus, to get the response of the excavation due to seismic event only (to simulate the experimental condition), all the responses generated during the static condition are nullified. However, the stresses generated by the Mohr-Coulomb model remain at the dynamic stage.

The 'Finn Model' is used to simulate the transient pore pressure generation properly within the soil during a dynamic loading as suggested by FLAC-2D (Itasca, 2005). The 'Finn model' is widely utilized to generate pore water pressure during liquefaction (Byrne, 1991; Martin *et al*., 1975). The 'Finn model' has been shown to capture the liquefaction of Kasai River sand by Banerjee *et al*. (2017). In the present analyses, undrained simulation is carried out where the mechanical responses are allowed under no flow condition. The changes in the pore water pressures are due to the volumetric strains only. Coupled, effective-stress analysis (with pore pressure measurements) approach is adopted in the numerical study, where all the drained properties of the sand are used (Itasca, 2005). The effective strength parameters (effective friction angle) are taken as the same in both drained (CD) and undrained (CU) conditions (Holtz and Kovacs, 1981). The changes in the pore water pressures in the 'Finn model' may be determined as (Banerjee *et al*., 2017):

$$\Delta u = M_s \Delta \varepsilon^p \tag{6}$$

where Δu is the change in the pore water pressures, M_s is the constrained modulus of the sand, $\Delta\varepsilon^p$ is the change in volumetric strains and given by $\gamma_s C_1 \exp(-C_2\varepsilon_{vd}/\gamma_s)]$, where ε_{vd} is the change in the volumetric strain. C_1 is a constant and given as $7600(D_r)^{-2.5}$. C_2 is another constant and given by $0.4/C_1$. D_r is the relative density of the soil and γ_s is the shear strain in the soil. As discussed earlier, the relative density (D_r) of the soil is maintained at 65% in the model test. The corresponding values of C_1, C_2 are calculated as 0.2231 and 1.79, respectively. For the 'Finn Model', the soil strength parameters are also kept the same as presented in Table 2. To check the performance of the 'Finn model' in accurately predicting the dynamic pore water pressures generated during the laboratory shake table test, a sinusoidal base acceleration of 0.2 g is applied to a uniform sand bed with the same spatial dimensions (800 mm × 800 mm with 400 mm height) and the pore water pressures are measured at 200 mm and 300 mm below the top. The pore water pressures predicted by the 'Finn model' are found to be close to the experimental data (as shown in Fig. 6).

The dynamic (mechanical) behavior of Kasai River sand is modeled by the modulus of the degradation curve. The cyclic tri-axial test (high strain) and the resonant column (low strain) test data for Kasai River sand obtained by Chattaraj and Sengupta (2016) at 100 kPa confining pressure are curve fitted using Eq. (7a) proposed by Hardin and Drnevich (1972) with the adjusting constants given by a=1.3 and b=1.0 (See Aggour and Zhang, 2006). Using Eq. (7a),the modulus degradation curve for Kasai River sand is obtained for the effective mean confining pressure of 1.16 kPa (for the small-scale model).

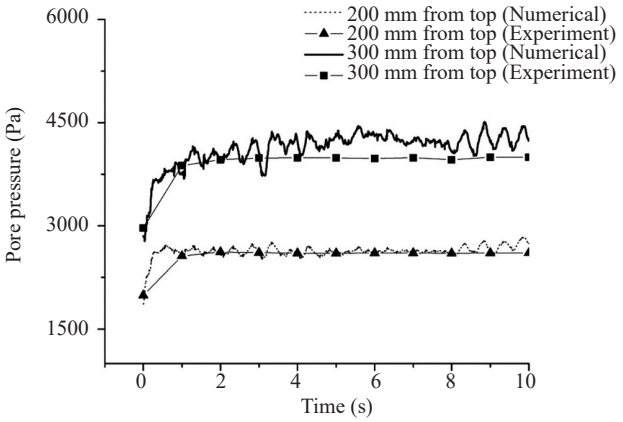

Fig. 6 Comparison of pore water pressures obtained from the numerical (using Finn Model) and the experimental studies

Table 2 Material parameters used for the numerical analyses of the braced excavation

Saturated unit weight of soil (kN/ m^3)	Friction angle (ϕ') (Degree)	Shear Modulus (G) of soil (kPa)	Poisson's ratio (μ_s) of soil	Stiffness of braced wall (EI) (N·m^2/m)	Stiffness of strut (EA) (N/m)
19.7	38°	1.66×10^3	0.3	7.29	9.12×10^5

$$M_e = G / G_{max} = 1/[1 + a(\gamma_e / \gamma_r)^b] \quad (7a)$$

where γ_e is a cyclic shear strain and γ_r is a reference shear strain in the soil. Ishabashi and Zhang (1993) have also proposed an equation (Eq. (7b)) for modulus reduction of soil considering the combined effect of plasticity index (*PI*) and different confining pressure (See Kramer, 1996). For Kasai River sand, the *PI* value is taken as zero. For an effective mean confining pressure (σ'_m) of 1.16 kPa, the modulus reduction curve for the present soil is given by Eq. (7b).

$$M_e = G / G_{max} = K(\gamma_e, PI) \cdot (\sigma'_m)^{m(\gamma_e, PI) - m_0} \quad (7b)$$

where

$$K(\gamma_e, PI) = 0.5\left\{1 + \tanh\left[\ln\left(\frac{0.000102 + n(PI)}{\gamma_e}\right)^{0.492}\right]\right\}$$

$$m(\gamma_e, PI) - m_0 = 0.272\left\{1 - \tan h\left[\ln\left(\frac{0.000556}{\gamma_e}\right)^{0.4}\right]\right\} \cdot \exp(-0.0145 PI^{1.3})$$

The "Sigmoidal (sig4)" model available in FLAC 2D (Itasca, 2005) expresses the degradation of the modulus of a soil with the shear strains by Eq. (7c). Figure 7 shows the model simulation in FLAC 2D using the "Sigmoidal" model for present confining pressure.

$$M_e = y_0 + \frac{a'}{1 + \exp\left[-(L - x_0)/b'\right]} \quad (7c)$$

where L is the logarithmic strain and given by $L = \log_{10}(\gamma_e)$, where γ_e is the cyclic shear strain in the soil. The parameters a', b', x_0 and y_0 are the parameters with the values of 0.96, -0.4, -2.0 and -0.03, respectively, corresponding to the best fit curve shown in Fig. 7. The soil behavior under cyclic loading can be represented by the relationship between M_e and γ_e (Itasca, 2005). The shear stress (τ) and the shear strain (γ_e) may be related under plane strain conditions as:

$$\frac{\tau}{G_0} = \frac{G_s(\gamma_e)}{G_0}\gamma_e = M_e(\gamma_e) \cdot \gamma_e \quad (8)$$

where $G_s(\gamma_e)$ is the secant shear modulus, G_0 is the small strain shear modulus and M_e is the normalized secant shear modulus.

5 Results and discussions

The responses of the instrumented braced wall, strut and the surrounding soil obtained from numerical analyses are compared with the corresponding shake table results. To measure the horizontal motions during a dynamic event in the experiments, accelerometers are attached to the shake table and also placed on the top of the ground surface behind the braced wall. For a given case, the same base motions, applied to the shake table, are also specified in the numerical analysis. Figure 4(b) shows a comparison between the base motions recorded at the base of the model test setup by accelerometer AC1 and those applied numerically in the numerical analysis for the case, BW2. The motions obtained from the accelerometer (AC2) at the top surface of the soil beside the braced excavation are also compared with the corresponding numerical results and presented in Fig. 4(a). As may be observed from Fig. 4, the ground motion is amplified by about 1.24 times at the top soil surface for a sinusoidal motion of 0.25 g with a frequency of 2 Hz and applied for 7 s. The numerically obtained motions are found to be comparable with the motions recorded during the tests. However, from the acceleration time histories at the top soil surface (both experimentally and numerically), no significant effect of liquefaction is observed.

Table 3 shows the measured (experimentally and numerically) static pore water pressures for different tests. No separate analytical values for pore water pressures are determined. However, the numerical values can be interpreted as analytical values. In the present study, as mentioned before, the proper construction sequence is not followed for the braced excavation construction. Therefore, the change in strain or deflection of the walls due to the excavation is not measured. Thus, static

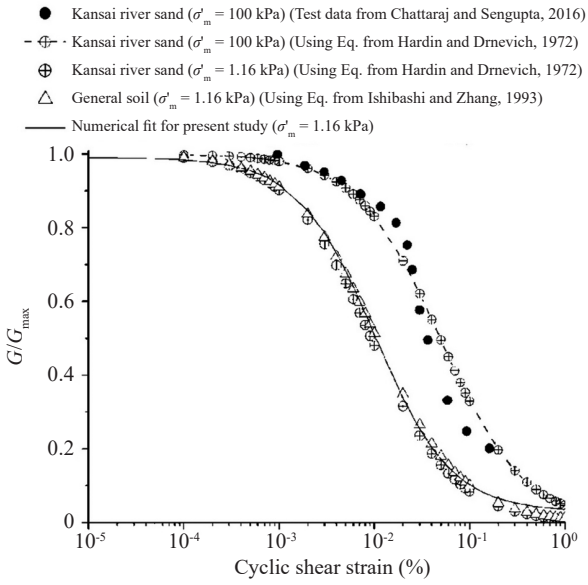

Fig. 7 Modulus of degradation curve for Kasai River sand

Table 3 Static pore water pressures (in Pa) obtained from the numerical and the experimental studies before the seismic event

Pore pressure transducers	Case	Normalized excavation depth (D_e/H)		
		0.4	0.5	0.6
PP1	Numerical	1647	1589	1507
	Experiment	1710	1662	1605
PP2	Numerical	1107	864	607
	Experiment	1080	918	778
PP3	Numerical	2286	2109	1929
	Experiment	2012	1762	1529

bending moment, lateral deformation and strut force are not measured. All the LVDTs, strain gauges data are recorded at the beginning and the end of the motions. The net bending moments, lateral deformations and strut forces are computed from the strain data after the motions. Note that the densification of the sand during saturation before the dynamic model test is ignored since the model test dimensions are small.

In saturated sand, excess pore water pressures develop during a seismic loading, which often cause soil liquefaction. The excess pore water pressures reduce the effective stresses in a soil, which may lead to greater damage to the structures located on the soil. When excess pore pressures developed in a soil are equal to the initial vertical effective stresses, a soil is considered to be fully liquefied. Three pore water pressure transducers (PP1, PP2 and PP3) are attached in three different positions in the test tank to measure the absolute pore water pressures developed during the model tests. Figure 8 shows the pore water pressure ratio, r_u, recorded with time by the transducers PP1, PP2 and PP3 during the test BW2. These values are compared with the corresponding numerically obtained values. The pore water pressure ratio is defined as the excess pore water pressure (Δu) developed in a soil divided by the initial vertical effective stress. It is found that the maximum values of pore water pressure ratios (r_u) in the soil below the excavation (at PP2, PP3) are much higher than those (PP1) values recorded by the sides of the walls and below the soil surface. Thus, in a braced excavation, the soil located below the excavation level is more susceptible to liquefaction. The soil below the excavation level bears the loads from the braced walls and provides stability to the excavated portion. Thus, higher values of pore water pressure below the excavation level could cause serious damage to the braced walls. In the small-scale test, the application of dynamic loading with peak amplitude 0.15 g to 0.35 g has caused generation of excess pore pressure from the initial loading stage itself, which has been reported by others as well (Wang *et al*., 2015; Khosrojerdi and Pak, 2015). However, for much smaller amplitude of loading, a gradual generation of the pore water pressure could have been observed, but such small amplitude of loading

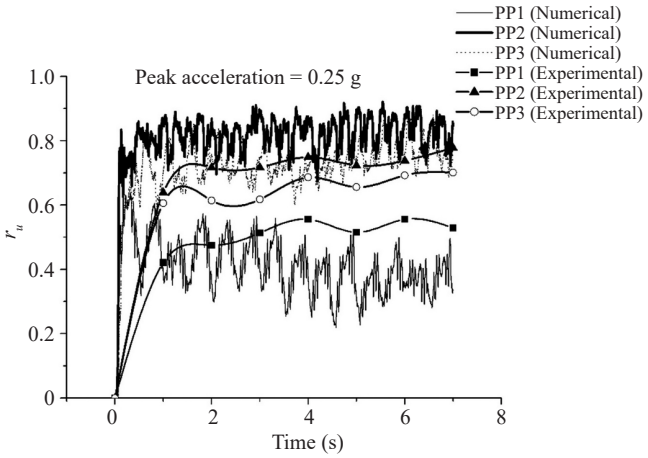

Fig. 8 Variation of pore water pressures ratio (r_u) with time in BW2 test

was not of interest in the present study. No significant change in the acceleration time history at the soil surface is observed corresponding to the changes in the pore water pressures in case of peak ground acceleration of 0.25 g. In the numerical modeling, the properties at the soil-structure interfaces are based on the recommendations provided by the FLAC 2D manual. These are general recommendations and may not accurately represent the actual interface behavior in the present situation. It is very difficult to estimate the properties at the actual soil-structure interface. In the present case, the guidelines provided by FLAC 2D are adopted to come up with the interface properties. The use of the hyperbolic model and the pore water pressure generation model also has some shortcoming in modeling the complications arising during soil liquefaction. Under a dynamic condition, fluctuations in the pore water pressures are normal. However, this fluctuation in the pore water pressures in the soil is not captured in the shake table tests as the pore water pressures are measured at 1s intervals due to the limitation of the data acquisition system. Thus, the pore water pressures measured during the model tests give a general trend of its variations. However, in the numerical analyses, the chosen time step is 2.56×10^{-5} s to ensure convergence. Thus, 39062 data points per

second are taken for the pore water pressures in the numerical analysis. The numerical results show the fluctuations in the pore water pressures in the soil with the dynamic loadings as depicted in Figs. 8–10. Due to these various reasons, the differences between the experimental observations and the numerical results have been observed in the present study.

To observe the effects of peak amplitude of the ground motions on the generation of the pore pressures in soil around a braced excavation, development of the pore water pressure ratios (r_u) at PP3 with time as observed in the shake table tests and the corresponding numerically obtained values are compared in Fig. 9. The depth of the excavations is kept the same at $D_e/H = 0.5$ for all the cases, where D_e is the excavation depth and H is the height of the retaining walls. Figure 9 shows that the pore water pressure ratios (r_u) developed in the soil are greater when the amplitudes of the motions are increased. For the 0.15 g motion, the developed pore pressures in the soil are less than unity and the soil does not liquefy. However, for the peak amplitudes of 0.25 g and 0.35 g, the soil is close to the liquefaction state near the excavation bottom.

The changes in the pore pressures ratios (r_u) are also investigated for different excavation depths (D_e/H). In these cases, the amplitude of the base motions is kept the same at 0.25 g. The different normalized excavation depths (D_e/H) considered in this study are 0.4, 0.5 and 0.6. The pore water pressure values with time at PP3 for different normalized excavation depths (D_e/H) are shown in Fig. 10. The figure shows that the pore water pressure ratios (r_u) increase with the increase in D_e/H. For $D_e/H = 0.4$, the soil does not liquefy. However, for $D_e/H = 0.5$, the soil is closer to liquefaction. For $D_e/H = 0.6$, the soil is liquefied as the pore water pressures ratio (r_u) reaches close to the unity. Throughout the model tests, the water table outside the excavation is maintained by pumping water into the test chamber from the top. Within the excavated portion between the two braced walls, the water table is maintained just below the excavation level by pumping out water from the excavation. Thus, as the depth of excavation increases, the effective stresses within the soil below the excavation decrease, increasing the potential of liquefaction in the sandy soil below the excavated portion. Thus, the liquefaction potential of a soil (below the excavation) increases as the depth of excavation between the braced walls increases, provided the soil is liquefiable as in the present case.

The displacement of a wall at the end of a seismic event is one of the performance indicators for a retaining wall (Richards and Elms, 1979). The lateral displacements of the right wall observed in the shake table tests are compared with the corresponding numerically obtained values for different base motions and different excavation depths (D_e), and presented in Fig. 11. It is found that these two parameters have great influence on the lateral displacements of a braced wall embedded in saturated sand. The lateral displacements (u) of the right wall obtained from the experimental and numerical studies under different peak amplitudes (0.15 g, 0.25 g and 0.35 g) of the base motions and for a given excavation depth, D_e/H=0.5, are presented in Fig. 11(a). The numerical results show significant lateral displacements of the wall at the top, with the hinge point (point of rotation of the wall) around 0.32 d/H for the peak acceleration of 0.35 g. However, experimental results show that the hinge point is developed nearly at 0.15 d/H for the same case. For the cases of 0.15 g and 0.25 g, the hinge points are close to the top surface from both experimental and numerical studies. For peak acceleration 0.35 g, the soil below the excavation liquefies as the pore pressure ratio (r_u) at PP2 reaches unity (as shown in Fig. 9). In this liquefied state, a soil has very small shear strength and it flows like fluid which causes large deformation and rotation of the walls. Thus, differences between the experimental and the numerical results are observed at this stage due to involvement of approximations in the numerical analyses to model the complications and unpredictability arising

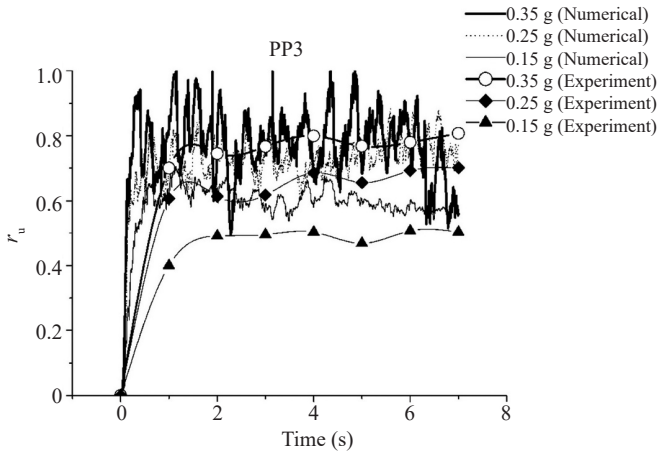

Fig. 9 Variation of pore water pressures ratio (r_u) at PP3 developed during earthquake with time for different peak amplitudes of base motions

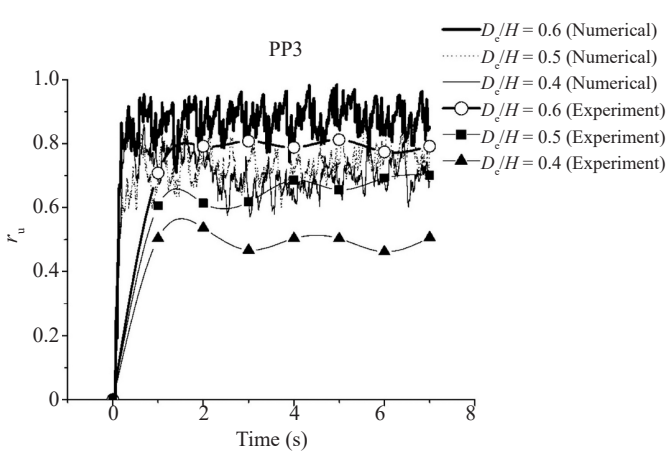

Fig. 10 Variation of pore water pressures ratio (r_u) at PP3 developed during earthquake with time for different excavation depths

during soil liquefaction. The soil below the excavation provides passive earth pressures on the wall which act as resistive forces against the wall movement. Thus, the shear strengths of the soil below the excavation level control the behavior of the braced wall. In the case of small peak amplitude of base acceleration, the soil below the excavation level does not liquefy, hence gives more resistance against the rotation and/or displacement of the wall. Thus, small lateral displacement and a small amount of rotation are observed in the wall. However, in the case of higher peak amplitude of base motion (0.35 g), the soil below the excavation liquefies and it provides less resistance against rotation and/or deformation. Therefore, large displacement and rotation in the wall is observed for these cases and the hinge point shifts in the downward direction.

The lateral displacements (u) of the right wall obtained from the experimental and numerical studies under different normalized excavation depths (D_e/H) of 0.4, 0.5 and 0.6 are presented in Fig. 11(b). The peak amplitude of the motions is kept the same at 0.25 g in these cases. From the numerical analyses, it may be seen that in all these cases, the maximum lateral displacements of the walls occur near the bottom. The maximum normalized lateral displacement (u/H) of the right wall at different normalized excavation depths (D_e/H) of 0.4, 0.5 and 0.6 is 0.0327, 0.0432 and 0.1578, respectively. For the case of D_e/H = 0.4, the lateral displacement of the wall is less with the increment of the depth of embedment as greater resistance is offered by the wall against the lateral displacement. For the case of D_e/H =0.4, the developed pore water pressures within the soil are less than that for the case of D_e/H =0.5 and 0.6 (see Fig. 10). Thus, the larger excavation depth (D_e/H) is not only decreases the embedment depth of the walls, but also increases the possibility of liquefaction of the soil. Large lateral displacements of the walls are observed as the depth of excavation and the amplitude of the base motions are increased simultaneously.

The distributions of the bending moment (M) (expressed in the normalized form as $M/\gamma'H^3$, with γ'= effective unit weight of the sand used in these experiments and H= total depth of the braced walls) on the right braced wall under different peak amplitudes of the base motions and different excavation depths, obtained from the numerical analyses and the shake table tests, are compared in Figs. 12(a) and 12(b). It is found that for a single strut braced excavation, the maximum bending moment develops near the bottom of the excavation. It is also observed from the numerical analyses that as the magnitude of the base motions is increased from 0.15 g to 0.25 g, the maximum moment ($M/\gamma'H^3$) increases by 67%. However, the maximum moment ($M/\gamma'H^3$) in the wall is changed by only 23% as the magnitude of the motions is increased further from 0.25 g to 0.35 g. Due to the increase in the amplitude of the base motions, a larger force is applied to the braced wall, which produces larger moments until the surrounding soil liquefies. However, as the magnitude of the base motions is increased further from 0.25 g to 0.35 g, the soil liquefies and the braced walls start to float in the liquefied soil. At this stage, the braced walls undergo large deformations due to rotations, but at the same time, the local strains are not increased significantly causing less increment of moments. Similarly, when the depth of excavation, D_e/H, is increased from 0.4 to 0.5, the maximum moment ($M/\gamma'H^3$) in the wall is increased by 51%. However, as the depth of excavation between the walls (D_e/H) is increased further from 0.5 to 0.6, the maximum moment ($M/\gamma'H^3$) in the wall increases by about 54%. The increase in the excavation depth (D_e/H) between the braced walls induces liquefaction at a faster

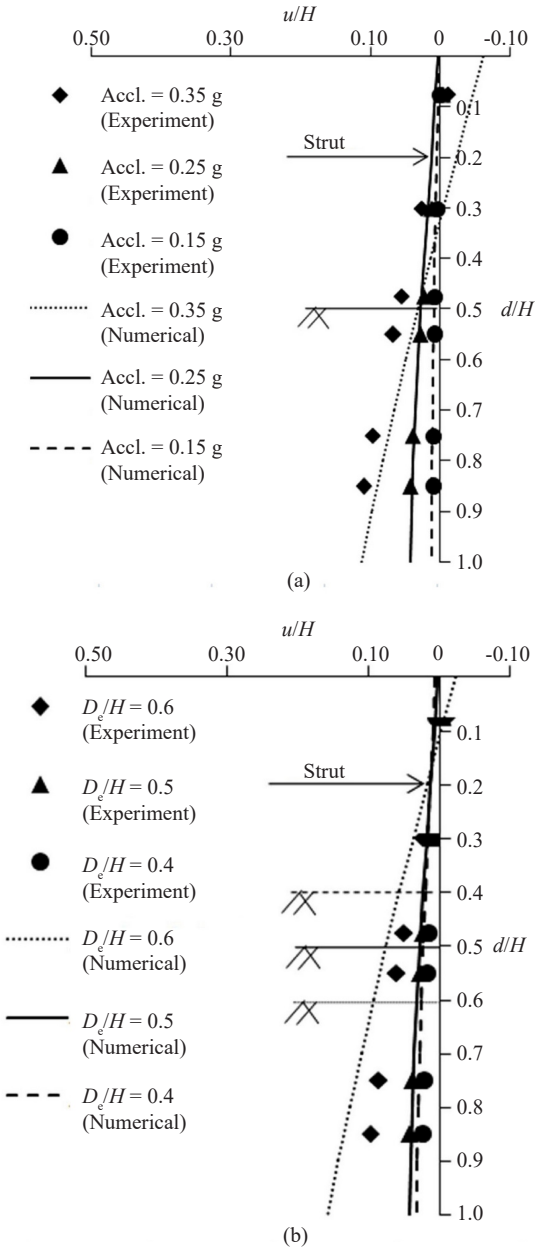

Fig. 11 Lateral displacements (u/H) of the braced wall for (a) different peak amplitude of the base motions, (b) different excavation depths (D_e/H)

rate and as explained above, as the surrounding soil liquefies, the braced walls undergo large rotations.

In the shake table experiments, only one level of struts are used. A number of strain gauges are glued to the struts to obtain the axial force on the strut during the dynamic loadings. The strut force (F), in a normalized form (F/E_pA) is reported here, with E_p= elastic modulus of the strut material (plexiglass) and A= cross-sectional area of the strut. The value of E_pA is 9.12×10^5 N/m. The strut forces obtained from the numerical analyses and the corresponding shake table tests are shown in Table 4. The numerical results indicate that the strut forces (F/E_pA) increase by 52%, when the magnitude of the base motions is increased from 0.15 g to 0.25 g. However, they decrease by 12% when the amplitude is increased further from 0.25 g to 0.35 g. For the amplitude of the base motions as 0.35 g, the surrounding soil liquefies and the bracing system fails completely releasing the forces in the struts. The strut forces are increasing by 18% and 42% as the excavation depth (D_e/H) is increased from 0.4 to 0.5 and 0.5 to 0.6, respectively.

Figure 13 shows the changes in the pore water pressures with time when the applied base motion is stopped. It is observed that due to a higher value of permeability of the sand, the pore pressures developed during the motions dissipate as soon as the base motion ceases. The residual bending moments, lateral deformations are not measured during this short duration. However, studies (Boulanger *et al*., 2003; Moghadam *et al*., 2011) show that the structural responses after the dissipation of the pore water pressures are not critical and do not change with time. The numerically obtained responses of the braced excavation during the dynamic

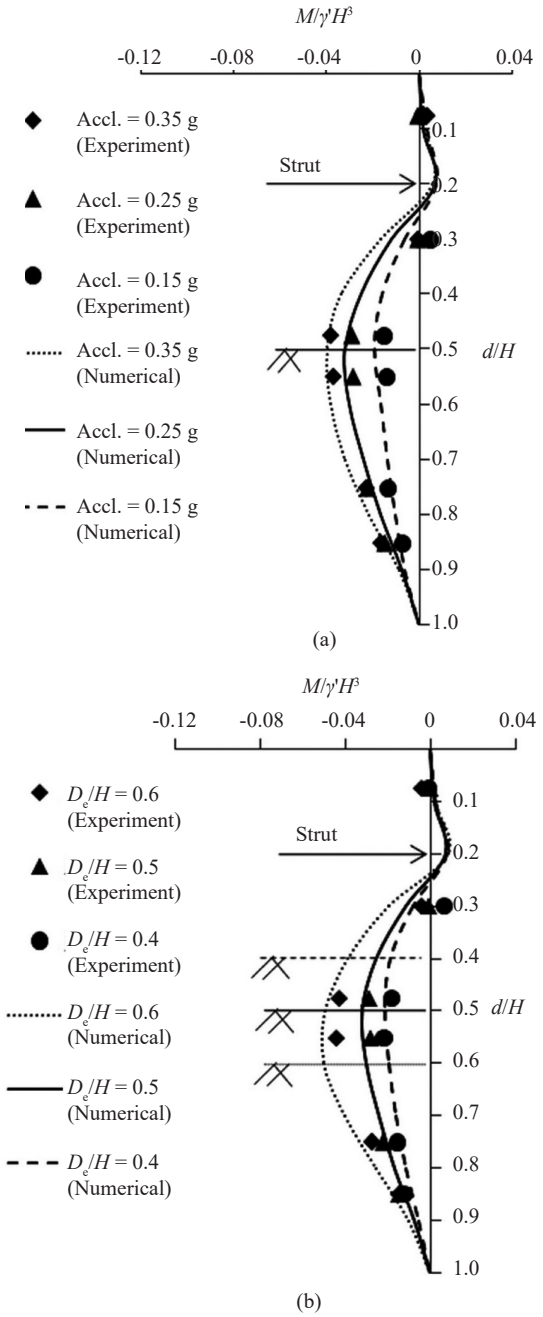

Fig. 12 Bending moments ($M/\gamma'H^3$) in the braced wall for (a) different peak amplitudes of the base motions, (b) different excavation depths (D_e/H)

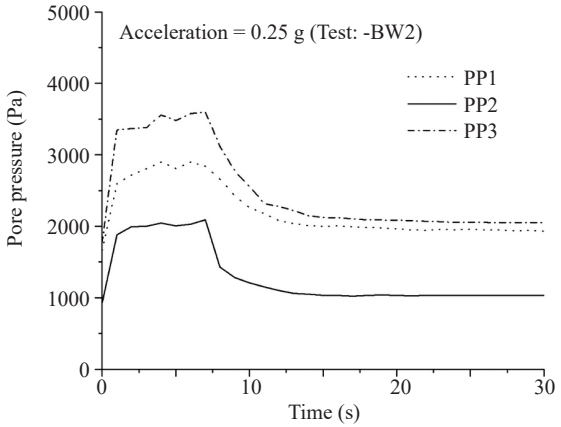

Fig. 13 Variation of total pore water pressures with time obtained from BW2 model shake table test

Table 4 Normalized strut forces (F/E_pA) ($\times10^{-5}$) with varying peak amplitudes of the base acceleration and normalized excavation depths (D_e/H)

Case	Peak acceleration (g)			Normalized excavation depth (D_e/H)		
	0.15	0.25	0.35	0.4	0.5	0.6
Numerical	3.50	5.33	4.69	4.50	5.33	7.57
Experimental	4.46	6.06	6.00	5.17	6.06	7.40

event are presented for different peak magnitudes of the base motions and different excavation depths. The bending moments and lateral deformations in the wall and the strut forces during the motions are presented in Figs. 14(a), 14(b) and in Figs. 15(a), 15(b). It is observed that for lower depth of excavation (0.4 and 0.5) and lower peak amplitudes of base motions (0.15 g and 0.25 g), the bending moments increase with time (see Figs.14(a) and 14(b)). However, in the case of peak acceleration of 0.35 g (see Fig. 14(a)), a sudden change in the value of the bending moment over the time is observed. A sudden rise in the bending moment during the very early stage of the loading is also observed for D_e/H=0.6. From Figs. 15(a), it is observed that the lateral displacements of the wall gradually changes with duration for different values of peak accelerations. For lower acceleration amplitudes, large variation in strut force with time is not observed, but as the liquefaction occurs in higher peak acceleration, significant variation in strut force with time is observed (see Fig. 15(b)).

6 Conclusions

The performance of a braced wall embedded in saturated sand is investigated experimentally on a shake table and numerically at different amplitudes of the base motions and for different excavation depths. One layer of bracing is considered in the study. The material properties of the structures and the soil, excavation width and relative density of the soil are kept identical in all the cases. The experimental and numerical results are compared and show reasonably good agreement for all the cases. Higher excess pore water pressures are found to develop in the soil below the excavation as compared to those on the sides and away from the braced walls. This indicates that the soil below the bottom of the excavation is more susceptible to liquefaction due to a high gradient of seepage pressures that develope due to dewatering of the excavated area. Thus, during the design process, one needs to pay more attention to the liquefaction prevention and/or prevention of built-up of pore water pressures near the bottom of a braced excavation. It is also found from the study that the pore water pressure ratios (r_u) increase with increasing peak amplitude of the base motions. The increase in the depth of excavation (D_e) also helps in initiating liquefaction in a braced excavation. For a given depth of excavation (D_e/H), the lateral displacements (u) and the bending moments (M) in the braced walls increase with the magnitude of the base motions. However, when the soil liquefies due to the increase in the magnitude of the base

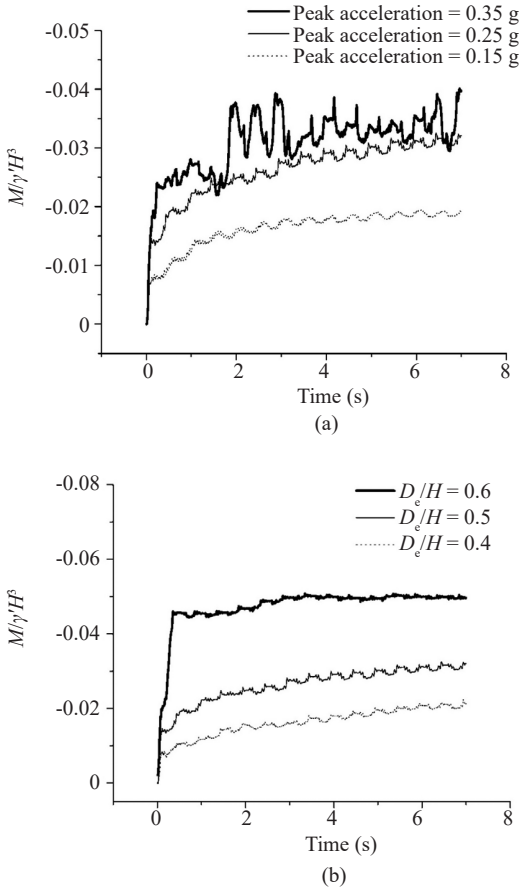

Fig. 14 Time histories for maximum bending moment of the wall ($M/\gamma'H^3$) under different (a) peak amplitudes of base acceleration (b) excavation depths (D_e/H)

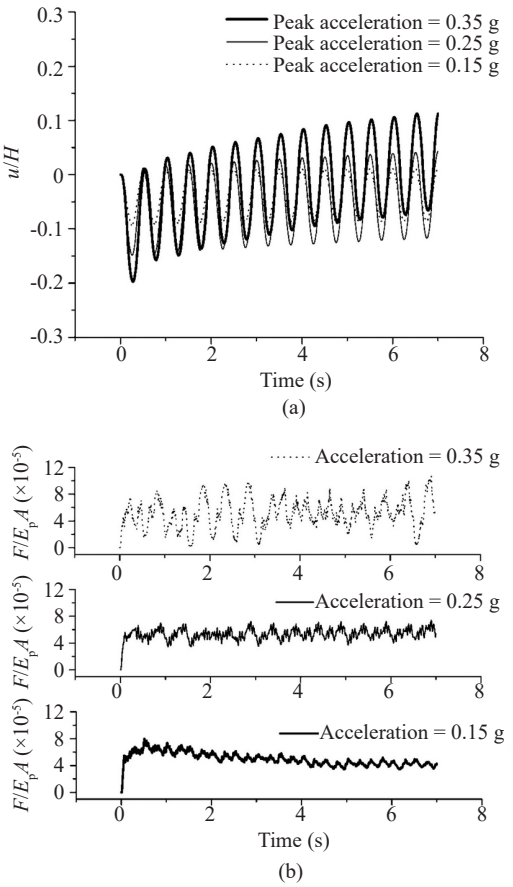

Fig. 15 Time histories for (a) maximum lateral displacement of the wall (u/H) and (b) axial force developed in the strut under different peak amplitudes of base acceleration

motions, the braced walls undergo large deformations due to rotations without a significant increment in the local strains, causing less increment of bending moments. For a given amplitude of the base motions, the lateral displacements (u) and the bending moments (M) in the braced walls increase with the depth of excavation (D_e/H). For both higher and lower amplitudes of base accelerations, the lateral displacements during and at the end of the dynamic events remain the same.

Acknowledgement

The funding for this study. provided by grant No. SR/S3/MERC-0029/2011 of SERB, Department of Science & Technology, New Delhi (India), is gratefully acknowledged.

References

Aggour MS and Zhang JX (2006), "Degradation of Sands due to Combined Sinusoidal Loading," *Journal of Geotechnical and Geoenvironmental Engineering*, **132**(12): 1628–1632.

Aminpour MM, Maleki M and Ghanbari A (2018), "Predicting Seismic Permanent Displacement of Soil Walls under Surcharge Based on Limit Analysis Approach," *Earthquake Engineering and Engineering Vibration*, **17**(4): 747–759.

Bandyopadhyay S, Sengupta A and Reddy GR (2015), "Performance of Sand and Shredded Rubber Tire Mixture as a Natural Base Isolator for Earthquake Protection," *Earthquake Engineering and Engineering Vibration*, **14**(4): 683–693.

Banerjee R, Konai S, Sengupta A and Deb K (2017), "Shake Table Tests and Numerical Modeling of Liquefaction of Kasai River Sand," *Geotechnical and Geological Engineering*, **35**(4): 1327–1340.

Bose SK and Som NN (1998), "Parametric Study of a Braced Cut by Finite Element Method," *Computers and Geotechnics*, **22**(2): 91–107.

Boulanger RW, Kutter BL, Brandenberg SJ, Singh P and Chang D (2003), "Pile Foundations in Liquefied and Laterally Spreading Ground during Earthquakes: Centrifuge Experiments and Analyses," *Report No. UCD/CGM-03/01*, Department of Civil and Environmental Engineering, College of Engineering, University of California at Davis, USA.

Byrne PM (1991), "A Cyclic Shear-Volume Coupling and Pore-Pressure Model for Sand," *Proceedings of Second International Conference on Recent Advances in Geotechnical Earthquake Engineering and Soil Dynamics*, St. Louis, Missouri, USA, Paper No. 1.24: 47–55.

Callisto L and Soccodato FM (2007), "Seismic Analysis of an Embedded Retaining Structure in Coarse Grained Soils," *Proceeding of the Fourth International Conference on Earthquake Geotechnical Engineering*, Thessaloniki, Dordrecht, Netherlands, Springer.

Callisto L, Soccodato FM and Conti R (2008), "Analysis of the Seismic Behavior of Propped Retaining Structures," *Proc. of Geotechnical Earthquake Engineering and Soil Dynamics IV* GSP, **181**: 1–10.

Chattaraj R and Sengupta A (2016), "Liquefaction Potential and Strain Dependent Dynamic Properties of Kasai River Sand," *Soil Dynamics and Earthquake Engineering*, **90**: 467–475.

Chen YM, Zhang ZC and Liu HL (2017), "Study of the Seismic Performance of Hybrid A-Frame Micropile/MSE (Mechanically Stabilized Earth) Wall," *Earthquake Engineering and Engineering Vibration*, **16**(2): 275–295.

Chowdhury SS, Deb K and Sengupta A (2013), "Estimation of Design Parameters for Braced Excavation: A Numerical Study," *International Journal of Geomechanics*, **13**(3): 234–247.

Chowdhury SS, Deb K and Sengupta A (2015), "Behavior of Underground Retaining Structure under Seismic Condition," *Earthquakes and Structures*, **8**(5): 1147–1170.

Chowdhury SS, Deb K and Sengupta A (2016), "Effect of Fines on Behavior of Braced Excavation in Sand: Experimental and Numerical Study," *International Journal of Geomechanics*, **16**(1): 04015018-1–04015018-13.

Chowdhury SS, Deb K and Sengupta A (2017), "Estimation of Design Parameters for Braced Excavation in Clays," *Geotechnical and Geological Engineering: An International Journal*, **35**(2): 857–870.

Conti R, Madabhushi GSP and Viggiani MB (2012), "On the Behaviour of Flexible Retaining Walls under Seismic Action," *Geotechnique*, **62**(12): 1081–1094.

Dasgupta S, Narula PL, Acharyya SK and Banerjee J (2000), *Seismotectonic Atlas of India and Its Environs*, Geological Society of India, Kolkata, India.

Finno RJ, Harahap IS and Sabatini PJM (1991), "Analysis of Braced Excavations with Coupled Finite Element Formulations," *Computers and Geotechnics*, **12**(2): 91–114.

Finno RJ and Harahap IS (1991), "Finite Element Analysis of HDR-4 Excavation," *Journal of Geotechnical Engineering Division*, **117**(10): 1590–1609.

Giri D and Sengupta A (2009), "Dynamic Behavior of Small Scale Nailed Soil Slopes," *International Journal of Geotechnical and Geological Engineering*, **27**(6): 687–698.

Gu LL, Zhang F, Bao XH, Shi ZM, Ye GL and Ling XZ (2018), "Seismic Behavior of Breakwaters on Complex Ground by Numerical Tests: Liquefaction and Post Liquefaction Ground Settlements," *Earthquake Engineering and Engineering Vibration*, **17**(2): 325–342.

Gu Q, Liu YD, Lin Y and Liu C (2018), "Finite Element Response Sensitivity Analysis of Three-Dimensional Soil-Foundation-Structure Interaction (SFSI) Systems," *Earthquake Engineering and Engineering Vibration*, **17**(3): 555–566.

Ha IS, Olson SM, Seo MW and Kim MM (2011), "Evaluation of Liquefaction Resistance Using Shaking Table Tests," *Soil Dyn. Earthq. Eng*., **31**(4): 682–691.

Hardin BO and Drnevich VP (1972), "Shear Modulus and Damping in Soils," *Journal of Soil Mechanics and Foundation Division*, **98**(7): 667–692.

Holtz RD and Kovacs WD (1981), *Introduction to Geotechnical Engineering*, Prentice-Hall Publishing, USA.

Hsiung BCB (2009), "A Case Study of Behavior of Deep Excavation in Sand," *Computers and Geotechnics*, **36**(4): 665–675.

Iai S (1989), "Similitude for Shaking Table Tests on Soil-Structure-Fluid Model in 1g Gravitational Field," *Soils and Foundations*, **29**(1): 105–118.

IS:1893 (2002), "Indian Standard Criteria for Earthquake Resistant Design of Structures, Part 1-General Provisions and Buildings," *Fifth Revision, Bureau of Indian Standard*, New Delhi, India.

Ishibashi I and Zhang X (1993), "Unified Dynamic Shear Moduli and Damping Ratios of Sand and Clay," *Soils and Foundations*, **33**(1): 182–191.

Itasca (2005), *User's Guide for FLAC-2D*, Version 5.0, Itasca India Consulting, Nagpur, India.

Janbu N (1963), "Soil Compressibility as Determined by Oedometer and Triaxial Tests," *European Conference on Soil Mechanics & Foundation Engineering*, Wiesbaden, Germany, **1**: 19–25.

Karlsrud K and Andresen L (2005),"Loads on Braced Excavation in Soft Clay," *International Journal of Geomechanics*, **5**(2): 107–113.

Khosrojerdi M and Pak A (2015), "Numerical Investigation on the Behavior of the Gravity Waterfront Structures under Earthquake Loading," *Ocean Engineering*, **106**: 152–160.

Konai S, Sengupta A and Deb K (2017), "Effect of Excavation Depths on Ground Surface Settlement for Embedded Cantilever Retaining Structure due to Seismic Loading," *Procedia Engineering*, **199**: 2342–2347.

Konai S, Sengupta A and Deb K (2018), "Behavior of Braced Excavation in Sand under a Seismic Condition: Experimental and Numerical Studies," *Earthquake Engineering and Engineering Vibration*, **17**(2): 311–324.

Konai S, Sengupta A and Deb K (2020), "Seismic Behavior of Cantilever Wall Embedded in Dry and Saturated Sand," *Frontiers of Structural and Civil Engineering*, **14**(3): 690-705.

Koseki J, Munaf Y, Tatsuoka F, TateyamaM, Kojima K and Sato T (1998), "Shaking and Tilt Table Tests of Geosynthetic Reinforced Soil and Conventional Type Retaining Walls," *Geosynthetic International*, **5**(1–2): 73–96.

Kramer SL (1996), *Geotechnical Earthquake Engineering*, Pearson Education, New Delhi.

Kung GTC, Juang CH, Hsiao ECL and Hashash YMA (2007), "Simplified Model for Wall Deflection and Ground-Surface Settlement Caused by Braced Excavation in Clays," *Journal of Geotechnical and Geoenvironmental Engineering*, **133**(6): 731–747.

Liu GB, Ng CWW and Wang ZW (2005), "Observed Performance of a Deep Multi-Strutted Excavation in Shanghai Soft Clays," *Journal of Geotechnical and Geoenvironmental Engineering*, **131**(8): 1004–1013.

Lombardi D, Bhattacharya S, Scarpa F and Bianchi M (2015), "Dynamic Response of a Geotechnical Rigid Model Container with Absorbing Boundaries," *Soil Dynamics and Earthquake Engineering*, **69**: 46–56.

Long M (2001), "Database for Retaining Wall and Ground Movementsdue to Deep Excavations," *Journal of Geotechnical and Geoenvironmental Engineering*, **127**(3): 203–224.

Martin GR, Finn WDL and Seed HB (1975), "Fundamentals of Liquefaction under Cyclic Loading," *J. Geotech. Engg. Div.*, ASCE, **101**(5): 423–438.

Matsuo O, Tsutsumi T, Yokoyama K and Saito Y(1998), "Shaking Table Tests and Analyses of Geosynthetic-Reinforced Soil Retaining Walls," *Geosynthetic International*, **5**(1–2): 97–126.

Meymand PJ (1998), "Shaking Table Scale Model Tests of Nonlinear Soil-Pile-Superstructure Interaction in Soft Clay," *PhD Dissertation*, Civil and Environmental Engineering Department, U.C. Berkeley, USA.

Moghadam AM, Ghalandarzadeh A, Moradi M, Towhata I and Hajialikhani P (2011), "Displacement Reducer Fuses for Improving Seismic Performance of Caisson Quay Walls," *Bulletin of Earthquake Engineering*, **9**(4): 1259–1288.

Mullins JP, Arulanandan K, Mitchell JK, Chan CK and Seed HB (1977), "Effects of Sample Preparation on Sand Liquefaction," *J. Geotech. Eng. Div., ASCE*, **103**(2): 91–108.

Nakai T, Kawano H, Murata K, Banno M and Hashimoto T (1999), "Model Test and Numerical Simulation of Braced Excavation in Sandy Ground: Influences of Construction History, Wall Friction, Wall Stiffness, Strut Position and Strut Stiffness," *Soils and Foundations*, **39**(3): 1–12.

Pain A, Choudhury D and Bhattacharyya SK (2017), "Seismic Passive Earth Resistance Using Modified Pseudo-Dynamic Method," *Earthquake Engineering and Engineering Vibration*, **16**(2): 263–274.

Qiao L, Yuan C, Miyajima M and Zhai E(2008), "Shake Table Testing and FLAC Modeling of Liquefaction-Induced Slope Failure and Damage to Buried Pipelines,"

Geotechnical Earthquake Engineering and Soil Dynamics IV, May 18–22, Sacramento, California, United States.

Richards Jr R and Elms DG (1979), "Seismic Behavior of Gravity Retaining Walls," *Journal of Geotechnical and Geoenvironmental Engineering*, **105**(4): 449–464.

Tavakoli H, Kutanaei SS and Hosseini SH (2019), "Assessment of Seismic Amplification Factor of Excavation with Support System," *Earthquake Engineering and Engineering Vibration*, **18**(3): 555–566.

Tefera TH, Nordal S, Grande L, Sandven R and Emdal A (2006), "Ground Settlement and Wall Deformation from a Large Scale Model Test on as Single Strutted Sheet Pile Wall in Sand," *International Journal of Physical Modelling in Geotechnics*, **6**(2): 1–13.

Tricarico M, Madabhushi GSP and Aversa S (2016), "Centrifuge Modeling of Flexible Retaining Walls Subjected to Dynamic Loading," *Soil Dynamics and Earthquake Engineering*, **88**: 297–306.

Tsuchida H (1970), "Prediction and Counter Measure Against the Liquefaction in Sand Deposits," *Proceedings of the Seminar of the Port and Harbour Research Institute*, Ministry of Transport, Yokosuka, Japan, **3**: 1–3.

Wang ZW, Ng CWW and Liu GB (2005), "Characteristics of Wall Deflections and Ground Surface Settlements in Shanghai," *Canadian Geotechnical Journal*, **42**(5): 1243–1254.

Wang L, Chen G and Chen S (2015), "Experimental Study on Seismic Response of Geogrid Reinforced Rigid Retaining Walls with Saturated Backfill Sand," *Geotextiles and Geomembranes*, **43**(1): 35–45.

Wood DM (2004), *Geotechnical Modeling*, CRC Press, Taylor & Francis Group.

Xie LT, Yan P, Lu WB, Chen M and Wang GH (2018), "Comparison of Seismic Effects During Deep Tunnel Excavation with Different Methods," *Earthquake Engineering and Engineering Vibration*, **17**(3): 659–675.

Ye B, Ye G, Ye W and Zhang F (2013), "A Pneumatic Shaking Table and Its Application to a Liquefaction Test on Saturated Sand," *Nat. Hazards*, **66**(2): 375–388.

Zekri A, Ghalandarzadeh A, Ghasemi P and Aminfar MH (2015), "Experimental Study of Remediation Measures of Anchored Sheet Pile Quay Walls using Soil Compaction," *Ocean Engineering*, **93**: 45–63.

Zeng X (2005), "Effect of Liquefaction on Stability of Retaining Walls," *Earthquake Engineering and Soil Dynamics*, GSP, **133**: 1–15.

Zhao XF, Wang SG, Du DS and Liu WQ (2017), "Simplified Analysis of Frame Structures with Viscoelastic Dampers Considering the Effect of Soil-Structure Interaction," *Earthquake Engineering and Engineering Vibration*, **16**(1): 199–217.

Zhou YG, Sun ZB, Chen J, Chen YM and Chen RP (2017), "Shear Wave Velocity-Based Evaluation and Design of Stone Column Improved Ground for Liquefaction Mitigation," *Earthquake Engineering and Engineering Vibration*, **16**(2): 247–261.